

Diffusive Fizeau Drag in Spatiotemporal Thermal Metamaterials

Liujun Xu,^{1,2} Guoqiang Xu,¹ Jiping Huang^{1,2,*} and Cheng-Wei Qiu^{1,†}

¹Department of Electrical and Computer Engineering, National University of Singapore, Singapore 117583, Singapore

²Department of Physics, State Key Laboratory of Surface Physics, and Key Laboratory of Micro and Nano Photonic Structures (MOE), Fudan University, Shanghai 200438, China

 (Received 5 October 2021; accepted 10 March 2022; published 8 April 2022)

Fizeau drag means that the speed of light can be regulated by the flow of water, owing to the momentum interaction between photons and moving media. However, the dragging of heat is intrinsically elusive, due to the absence of momentum in thermal diffusion. Here, we design a spatiotemporal thermal metamaterial based on heat transfer in porous media to demonstrate the diffusive analog to Fizeau drag. The space-related inhomogeneity and time-related advection enable the diffusive Fizeau drag effect. Thanks to the spatiotemporal coupling, different propagating speeds of temperature fields can be observed in two opposite directions, thus facilitating nonreciprocal thermal profiles. The phenomenon of diffusive Fizeau drag stands robustly even when the direction of advection is perpendicular to the propagation of temperature fields. These results could pave an unexpected way toward realizing the nonreciprocal and directional transport of mass and energy.

DOI: 10.1103/PhysRevLett.128.145901

Light travels at different speeds along and against the flow of water, which was theoretically predicted by Fresnel [1] and experimentally verified by Fizeau [2]. This momentous discovery, generally referred to as Fizeau drag, has been well explained by relativistic kinematics. Similar effects have also been revealed in other moving [3,4] or spatiotemporal [5,6] media. Recently, two experimental studies have reported plasmonic Fizeau drag by the flow of electrons [7,8], which results from the nonlinear kinematics of drifting Dirac electrons.

On the other hand, diffusive systems can also exhibit wavelike behaviors [9–14], which provides the possibility to realize diffusive Fizeau drag. However, unlike the dragging of photons and polaritons by the momentum interaction [Figs. 1(a) and 1(b)], it is intrinsically challenging to drag the macroscopic heat by the biased advection [Fig. 1(c)]. Therefore, the forward and backward propagating speeds of temperature fields are always identical. Nevertheless, the amplitudes of temperature fields are different in opposite directions, due to the dissipative property of heat transfer [17,18]. Therefore, it is still an extremely challenging problem to realize diffusive Fizeau drag.

Here, we construct a spatiotemporal thermal metamaterial with space-related inhomogeneity and time-related advection, to uncover diffusive Fizeau drag in heat transfer [Fig. 1(d)]. Since the characteristic length of spatiotemporal modulation is much smaller than the wavelength of wavelike temperature fields, the proposed structure can be regarded as a metamaterial. Neither periodic inhomogeneity nor vertical advection alone contributes to the horizontal

nonreciprocity, but their synergistic effect can give rise to diffusive Fizeau drag. The underlying mechanism lies in the coupling between heat flux and temperature change rate, which can be regarded as the thermal counterpart of

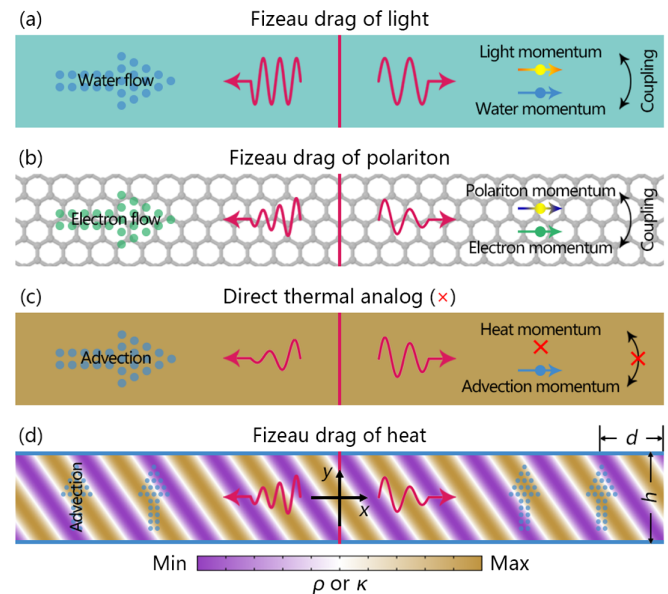


FIG. 1. Origin of diffusive Fizeau drag. Fizeau drag of (a) light and (b) polariton by the momentum interaction. (c) Failure of a direct thermal analog due to the lack of macroscopic heat momentum. (d) Fizeau drag of heat in a spatiotemporal thermal metamaterial by thermal Willis coupling. The red arrows contain the information of wave number and amplitude, indicating the forward and backward cases with (a),(b),(d) different wave numbers, and (c) different amplitudes.

Willis coupling in mechanical waves [19–23]. Therefore, the present nonreciprocity is distinctly different from the synthetic-motion-induced nonreciprocity [24,25].

We first explain why the direct scheme presented in Fig. 1(c) fails. Heat transfer in porous media is described by $\rho_0 \partial_t T + \nabla \cdot (\phi \rho_a \mathbf{u} T - \kappa_0 \nabla T) = 0$, where ρ_0 (or ρ_a) is the product of mass density and heat capacity of the porous medium (or fluid), κ_0 is the thermal conductivity of the porous medium, ϕ is the porosity, and \mathbf{u} is the velocity of the fluid with the horizontal and vertical components of u_x and u_y , respectively. We consider a wavelike temperature field described by $T = A e^{i(\beta x - \omega t)} + T_r$, where β and ω are the wave number and angular frequency, respectively. Here, we use “wavelike” because heat transfer is essentially governed by a diffusive equation rather than a wave equation. We set the temperature field amplitude of A as 1 and the balanced temperature of T_r as 0 for brevity. We apply a periodic source with a temperature of $T(x=0) = e^{-i\omega t}$, thus leading to a real ω and a complex β . The imaginary part of β reflects the spatial decay rate of wavelike temperature fields. We focus on the real part of β because the propagating speed of wavelike temperature fields can be calculated by $v = \omega/\text{Re}[\beta]$. The substitution of $T = e^{i(\beta x - \omega t)}$ with a preset real ω into the governing equation of heat transfer yields

$$\beta_{f,b} = \pm \frac{\sqrt{2}\gamma}{4\kappa_0} + i \frac{-8\phi\rho_a u_x \omega \rho_0 \kappa_0 \pm \sqrt{2}\gamma(2\phi^2 \rho_a^2 u_x^2 + \gamma^2)}{16\omega \rho_0 \kappa_0^2}, \quad (1)$$

where β_f and β_b are, respectively, the forward and backward wavenumbers with a definition of $\gamma = \sqrt{-\phi^2 \rho_a^2 u_x^2 + \sqrt{\phi^4 \rho_a^4 u_x^4 + 16\omega^2 \rho_0^2 \kappa_0^2}}$. Since a nonzero u_x cannot generate different $|\text{Re}[\beta]|$ in opposite directions, the forward and backward propagating speeds of temperature fields are identical, i.e., no diffusive Fizeau drag (see Supplemental Material, note I for detailed discussions [26]).

To achieve diffusive Fizeau drag, we introduce spatially-periodic inhomogeneity to the porous medium,

$$\rho(\xi) = \rho_0 [1 + \Delta_\rho \cos(G\xi + \theta)], \quad (2a)$$

$$\kappa(\xi) = \kappa_0 [1 + \Delta_\kappa \cos(G\xi)], \quad (2b)$$

where Δ_ρ and Δ_κ are the modulation amplitudes, $G = 2\pi/d$ is the modulation wave number, d is the horizontal modulation wavelength, $\xi = x + \zeta y$ is the generalized coordinate with a definition of $\zeta = d/h$, h is the vertical height, and θ is the modulation phase difference. To exclude the captivation that the horizontal advection can generate nonreciprocal amplitudes of temperature fields, as described by the imaginary part of Eq. (1), we consider the

upward advection with a speed of u_y , which does not contribute to the horizontal nonreciprocity. The governing equation of heat transfer in spatiotemporal thermal metamaterials can be expressed as

$$\bar{\rho}(\xi) \frac{\partial T}{\partial t} + \phi \epsilon u_y \frac{\partial T}{\partial y} + \frac{\partial}{\partial x} \left(-D_0 \bar{\kappa}(\xi) \frac{\partial T}{\partial x} \right) + \frac{\partial}{\partial y} \left(-D_0 \bar{\kappa}(\xi) \frac{\partial T}{\partial y} \right) = 0, \quad (3)$$

with definitions of $\bar{\rho}(\xi) = \rho(\xi)/\rho_0$, $\bar{\kappa}(\xi) = \kappa(\xi)/\kappa_0$, $\epsilon = \rho_a/\rho_0$, and $D_0 = \kappa_0/\rho_0$.

We further consider a wavelike temperature field with a spatially periodic modulation,

$$T = F(\xi) e^{i(\beta x - \omega t)} = \left(\sum_s F_s e^{isG\xi} \right) e^{i(\beta x - \omega t)}, \quad (4)$$

where $F(\xi)$ is a Bloch modulation function with parameters of $s = 0, \pm 1, \pm 2, \dots, \pm \infty$ and $F_0 = 1$. We can treat $e^{i(\beta x - \omega t)}$ as the temperature field envelope and $F(\xi)$ as local inhomogeneity. The substitution of Eq. (4) into Eq. (3) yields a series of component equations related to the order of s . For accuracy, we consider $s = 0, \pm 1, \pm 2, \dots, \pm 10$ and $F_{|s|>10} = 0$ to obtain twenty-one equations with twenty-one unknown numbers including β and $F_{|s|\leq 10}$, so β can be numerically calculated. The detailed derivations are presented in Supplemental Material, note II [26].

The properties of spatiotemporal modulation are reflected in three crucial dimensionless parameters of $2\pi\Gamma = \phi \epsilon u_y d / D_0$, $\Lambda = \Delta_\rho \cos \theta / \Delta_\kappa$, and $\zeta = d/h$. The parameter of $2\pi\Gamma$ is similar to the Peclet number, which can describe the ratio of advection to diffusion. The parameters of Λ and ζ reflect the influences of modulation amplitude and wavelength, respectively. We define the speed ratio as $\eta = |v_f/v_b| = |\text{Re}[\beta_b]/\text{Re}[\beta_f]|$ to discuss the degree of nonreciprocity, where v_f and v_b are the forward and backward propagating speeds of temperature fields, respectively.

We first discuss Λ when $\zeta = 0.2$ [Fig. 2(a)]. Since $2\pi\Gamma = 0$ and $2\pi\Gamma \rightarrow \infty$ always yield $\eta = 1$, it is necessary to introduce the vertical advection, but not the larger the better. Meanwhile, a speed difference still exists when $\Lambda = 0$ (i.e., $\Delta_\rho = 0$), so it is not necessary to modulate ρ and κ simultaneously. We find two types of curves in Fig. 2(a). Type I features that η is always larger than one (the top three curves). Type II features that η is first larger and then smaller than one (the bottom three curves). The transition between types I and II is at the critical point of $\Lambda = 1$ (the third curve from the top), where the modulations in Eqs. (2a) and (2b) do not affect the effective thermal diffusivity in the vertical direction (see Supplemental Material, note III for detailed

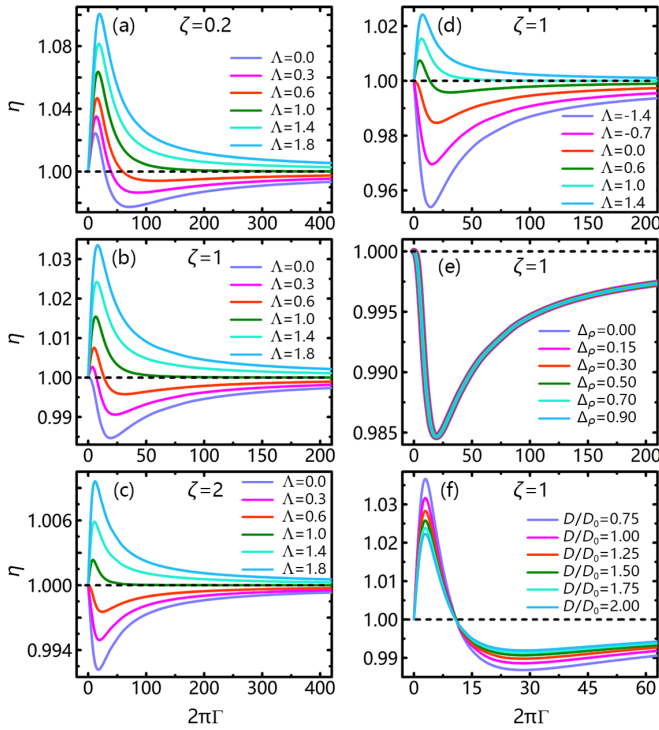


FIG. 2. Numerical results of the speed ratio of $\eta = |v_f/v_b|$ as a function of $2\pi\Gamma = \phi\epsilon u_y d/D_0$. $\Lambda = \Delta\rho \cos\theta/\Delta\kappa$ is tuned by (a)–(c) $\Delta\rho$ or (d) θ . Except the parameters presented in (a)–(f), the others are $\phi = 0.1$, $\epsilon = 1$, $D_0 = 5 \times 10^{-5} \text{ m}^2/\text{s}$, $d = 0.02 \text{ m}$, and $\omega = \pi/10 \text{ rad/s}$ for (a)–(f); $\Delta\rho = 0.7$ for (d); $\Delta\rho = 0.6$ for (f); $\Delta\kappa = 0.5$ for (a)–(e); $\Delta\kappa = 0.9$ for (f); $\theta = 0$ for (a)–(d) and (f); and $\theta = \pi/2$ for (e).

calculations [26]). When we change ζ from 0.2 to 1 [Fig. 2(b)] and 2 [Fig. 2(c)], type III curves appear, with η always smaller than 1. These three types indicate that nonreciprocal speeds can be flexibly manipulated.

We further discuss θ when $\zeta = 1$ [Fig. 2(d)], so $\Lambda = \Delta\rho \cos\theta/\Delta\kappa$ can be both positive and negative. The critical point of $\Lambda = 1$ still determines the transition between types I and II. Moreover, since $\theta = \pi/2$ always leads to $\Lambda = 0$, the curves in Fig. 2(e) are almost overlapped. We also discuss the thermal diffusivity of $D = \kappa/\rho$ [Fig. 2(f)], where κ is the balanced value of the periodic thermal conductivity and ρ is the balanced value of the periodic product of mass density and heat capacity. The peaks of η appear at almost the same value of $2\pi\Gamma$. Meanwhile, the peak of η gets larger as the thermal diffusivity decreases, which, however, does not mean that the smaller thermal diffusivity is the better. We do not discuss the small thermal diffusivity because the system becomes insulated.

We further plot the thermal dispersion in Fig. 3(a). The thermal dispersion curve is symmetric when $2\pi\Gamma = 0$, but becomes asymmetric when $2\pi\Gamma = 8$, which is the proof of diffusive Fizeau drag. We also plot the wave number difference $\Delta\text{Re}[\beta] = \text{Re}[\beta_f] + \text{Re}[\beta_b]$ in Fig. 3(b),

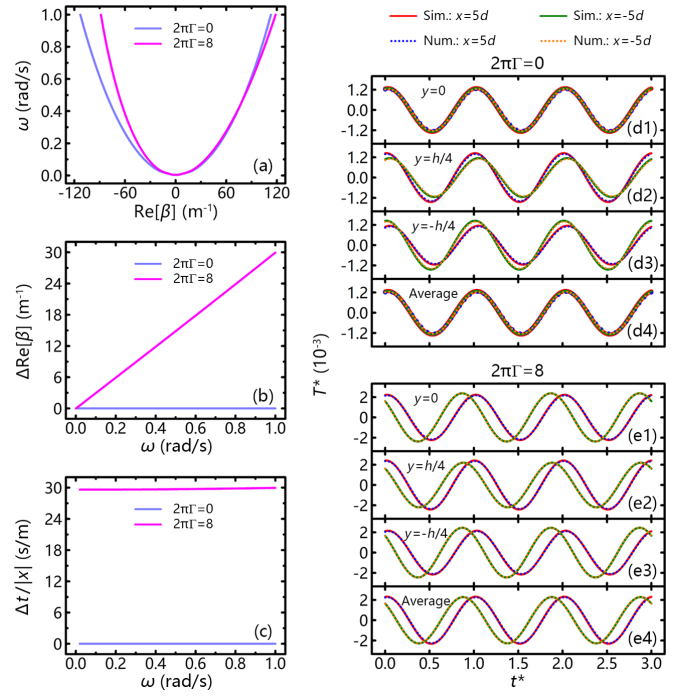


FIG. 3. Simulation results of diffusive Fizeau drag. (a) Thermal dispersion. (b) Wave number difference $\Delta\text{Re}[\beta] = \text{Re}[\beta_f] + \text{Re}[\beta_b]$ as a function of ω . (c) Time difference per unit of distance $\Delta t/|x| = \Delta\text{Re}[\beta]/\omega$ as a function of ω . Evolution of T^* when (d1)–(d4) $2\pi\Gamma = 0$ or (e1)–(e4) $2\pi\Gamma = 8$, corresponding to $u_y = 0$ or $u_y = 0.2 \text{ m/s}$, respectively. Parameters: $\phi = 0.1$, $\epsilon = 1$, $D_0 = 5 \times 10^{-5} \text{ m}^2/\text{s}$, $\Delta\rho = 0.9$, $\Delta\kappa = 0.9$, $\theta = \pi$, $d = 0.02 \text{ m}$, $h = 0.02 \text{ m}$, and $t_0 = 20 \text{ s}$. The simulation length is $30d = 0.6 \text{ m}$. The left and right boundaries are insulated. The upper and lower boundaries are set with periodic conditions. Simulation (Sim); Numerical (Num).

demonstrating linear responses to ω . More intuitively, a speed difference leads to a time difference of temperature field evolution at two symmetric positions of x and $-x$ to reach the same phases. The forward phase at x is $\text{Re}[\beta_f]x - \omega t_f$, and the backward phase at $-x$ is $-\text{Re}[\beta_b]x - \omega t_b$. The same phases correspond to a time difference of $\Delta t = t_f - t_b$, which can be calculated by

$$\Delta t = \Delta\text{Re}[\beta]|x|/\omega. \quad (5)$$

Since Δt increases linearly with $|x|$, we focus on the parameter of $\Delta t/|x| = \Delta\text{Re}[\beta]/\omega$ in Fig. 3(c), which is almost invariant as ω changes.

Finite-element simulations are also performed with COMSOL Multiphysics. For brevity, we define a dimensionless temperature of $T^* = (T - T_r)/A$ and a dimensionless time of $t^* = t/t_0$, where t_0 is the time periodicity of the temperature source. When $2\pi\Gamma = 0$ [Fig. 3(d1)], the forward and backward cases are identical at $y = 0$, but a slight difference appears at $y = \pm h/4$ [Figs. 3(d2) and 3(d3)] due to the local inhomogeneity

described by the $F(\xi)$ in Eq. (4). As long as we discuss the average temperature in the vertical direction, the effect of local inhomogeneity can be excluded, so the forward and backward cases become identical again [Fig. 3(d4)]. We further set $2\pi\Gamma = 8$, and the simulation results demonstrate a time difference of $\Delta t^* = 0.14$, which can be observed locally [Figs. 3(e1)–3(e3)] and globally [Fig. 3(e4)]. The numerical results predict a time difference of $\Delta t^* = 0.15$, indicating that the numerical calculations are convincing. Meanwhile, we plot the numerical results with dotted curves, which agree well with the simulation results.

To reveal the underlying mechanism of diffusive Fizeau drag, we analytically homogenize the governing equation (see Supplemental Material, note IV for detailed derivations [26]). We find two high-order terms of ∂_t^2 and $\partial_t \partial_x$ in the homogenized equation. This situation has a similarity to the properties of Willis metamaterials that result from the homogenization of inhomogeneous media [19–23]. The modified constitutive relation describing the heat flux of J can be approximately expressed as $\tau \partial_t J + J = -\kappa_e \partial_x T_0 + \sigma_2 \partial_t T_0$, where τ , κ_e , σ_2 , and T_0 are the homogenized parameters. Clearly, besides the temperature gradient of $\partial_x T_0$, the horizontal heat flux is also coupled with the temperature change rate of $\partial_t T_0$, which can be referred to as the thermal Willis term. Moreover, the thermal Willis term can lead to nonreciprocal $|\text{Re}[\beta]|$, but cannot generate nonreciprocal $|\text{Im}[\beta]|$. This property indicates an obvious speed difference but no amplitude difference in opposite directions, which agrees with the simulation results in Figs. 3(e1)–3(e4).

Inhomogeneity is crucial to thermal Willis coupling. When we consider only the horizontal inhomogeneity [Figs. 4(a1) and 4(a2)] or only the vertical inhomogeneity [Figs. 4(b1) and 4(b2)], thermal Willis coupling will disappear. We further change the modulations from cosine functions to square wave functions denoted by Π . When the periodicity of inhomogeneity is the same as that in Fig. 3(e)

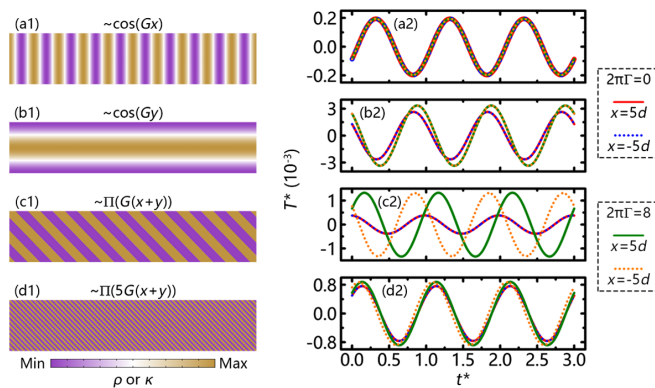


FIG. 4. Influences of inhomogeneity on thermal Willis coupling. The left column shows different kinds of inhomogeneity. The right column shows the evolution of T^* . The parameters and boundary conditions are the same as those in Fig. 3.

and $2\pi\Gamma = 8$, a time difference of $\Delta t^* = 0.32$ can be observed [Figs. 4(c1) and 4(c2)]. Therefore, the square wave modulation is more efficient than the cosine modulation ($\Delta t^* = 0.14$). We further reduce the modulation wavelength by a factor of five [Fig. 4(d1)]. When $2\pi\Gamma = 8$, a time difference of $\Delta t^* = 0.04$ appears, but it is far smaller than that of $\Delta t^* = 0.32$ in Fig. 4(c2). Therefore, the more homogeneous parameters yield weaker thermal Willis coupling, which is consistent with the existing understanding in mechanical waves [19–23].

For experimental suggestions, we design a three-dimensional structure without fluids, i.e., a three-layer solid pipe [Figs. 5(a) and 5(b)]. The inner and outer layers are homogeneous with the same angular velocities of Ω . The center layer is stationary with spatially periodic parameters of $\rho(\xi') = \rho_0[1 + \Delta_\rho \cos(G\xi' + \theta)]$ and $\kappa(\xi') = \kappa_0[1 + \Delta_\kappa \cos(G\xi')]$, where $\xi' = x + \alpha/G$ is the generalized coordinate in three dimensions with definitions of $\cos \alpha = z/\sqrt{y^2 + z^2}$ and $\sin \alpha = y/\sqrt{y^2 + z^2}$. The two rotating layers can provide the surface advection to the center layer, which has a similar effect as the bulk advection. The simulation results without and with angular rotation are presented in Figs. 5(c1)–5(c4) and 5(d1)–5(d4), respectively. The detecting locations are in the inner layer, center layer, outer layer, and all layers, respectively. Clearly, with proper angular rotation, a time difference between the forward and backward temperature field evolution appears, which is the direct indication of diffusive Fizeau drag.

Moreover, we can also generate a wavelike temperature field by setting an initial temperature of $T(t=0) = e^{i\beta x}$, thereby yielding a real β and a complex ω . To some extent, this case shows a duality to diffusive Fizeau drag (see Supplemental Material, note V for detailed discussions [26]).

Finally, we conclude the distinctive features of diffusive Fizeau drag. (I) As described by Eq. (1), only the biased advection cannot realize diffusive Fizeau drag. (II) Diffusive Fizeau drag in spatiotemporal thermal metamaterials results from thermal Willis coupling between heat flux and temperature change rate. (III) Diffusive Fizeau drag is unexpected because the vertical advection is generally unable to induce the horizontal nonreciprocity. (IV) Three types of curves in Fig. 2 indicate that diffusive Fizeau drag can be flexibly controlled.

In summary, we have revealed diffusive Fizeau drag in a spatiotemporal thermal metamaterial, featuring a speed difference of temperature field propagation in opposite directions. Spatial or temporal modulation alone cannot realize the horizontal nonreciprocity, so spatiotemporal modulation necessarily introduces the high-order coupling, which can be referred to as thermal Willis coupling between heat flux and temperature change rate. Diffusive Fizeau drag has also been visualized by observing the time difference of temperature field evolution at two symmetric

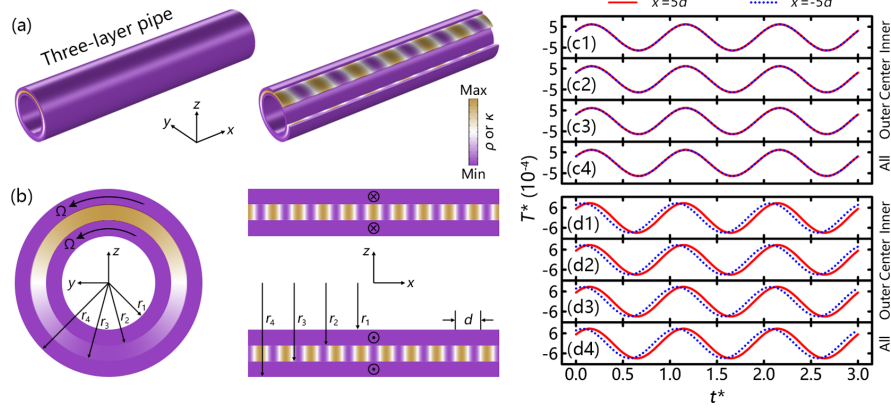


FIG. 5. Experimental suggestions. (a) Three-dimensional and (b) two-dimensional diagrams of a three-layer pipe. Temperature evolution when (c1)–(c4) $\Omega = 0$ or (d1)–(d4) $\Omega = 2\pi$ rad/s. The parameters of the center layer are $\rho_0 = 2 \times 10^6 \text{ J m}^{-3} \text{ K}^{-1}$, $\kappa_0 = 200 \text{ W m}^{-1} \text{ K}^{-1}$, $\Delta_\rho = 0.9$, $\Delta_\kappa = 0.9$, and $\theta = \pi$. Those of the inner and outer layers are $\rho = 2 \times 10^6 \text{ J m}^{-3} \text{ K}^{-1}$ and $\kappa = 10 \text{ W m}^{-1} \text{ K}^{-1}$. The other parameters are $d = 20 \text{ mm}$, $r_1 = 2.43 \text{ mm}$, $r_2 = 2.93 \text{ mm}$, $r_3 = 3.43 \text{ mm}$, $r_4 = 3.93 \text{ mm}$, and $t_0 = 20 \text{ s}$. The simulation length is $15d = 300 \text{ mm}$. The left and right boundaries are insulated.

positions. These results not only suggest a distinct mechanism to achieve nonreciprocal diffusion [30–32] by thermal Willis coupling but also have potential applications for controlling nonequilibrium heat and mass transfer [33–35].

C.-W. Q. acknowledges the support from the Ministry of Education, Singapore (Grant No.: A-0005143-00-00 | R-263-000-E19-114). J. H. acknowledges the support from the National Natural Science Foundation of China (Grants No. 11725521 and No. 12035004) and the Science and Technology Commission of Shanghai Municipality (Grant No. 20JC1414700).

*jphuang@fudan.edu.cn

[†]chengwei.qiu@nus.edu.sg

- [1] A. Fresnel, *Ann. Chim. Phys.* **9**, 57 (1818).
- [2] H. Fizeau, *C. R. Acad. Sci.* **33**, 349 (1851).
- [3] P.-C. Kuan, C. Huang, W. S. Chan, S. Kosen, and S.-Y. Lan, *Nat. Commun.* **7**, 13030 (2016).
- [4] T. Qin, J. F. Yang, F. X. Zhang, Y. Chen, D. Y. Shen, W. Liu, L. Chen, X. S. Jiang, X. F. Chen, and W. J. Wan, *Commun. Phys.* **3**, 118 (2020).
- [5] P. A. Huidobro, E. Galiffi, S. Guenneau, R. V. Craster, and J. B. Pendry, *Proc. Natl. Acad. Sci. U.S.A.* **116**, 24943 (2019).
- [6] P. A. Huidobro, M. G. Silveirinha, E. Galiffi, and J. B. Pendry, *Phys. Rev. Applied* **16**, 014044 (2021).
- [7] Y. Dong, L. Xiong, I. Y. Phinney, Z. Sun, R. Jing, A. S. McLeod, S. Zhang, S. Liu, F. L. Ruta, H. Gao, Z. Dong, R. Pan, J. H. Edgar, P. Jarillo-Herrero, L. S. Levitov, A. J. Millis, M. M. Fogler, D. A. Bandurin, and D. N. Basov, *Nature (London)* **594**, 513 (2021).
- [8] W. Y. Zhao, S. H. Zhao, H. Y. Li, S. Wang, S. X. Wang, M. I. B. Utama, S. Kahn, Y. Jiang, X. Xiao, S. Yoo, K. Watanabe, T. Taniguchi, A. Zettl, and F. Wang, *Nature (London)* **594**, 517 (2021).
- [9] M. Farhat, S. Guenneau, P.-Y. Chen, A. Alù, and K. N. Salama, *Phys. Rev. Applied* **11**, 044089 (2019).
- [10] M. Gandolfi, C. Giannetti, and F. Banfi, *Phys. Rev. Lett.* **125**, 265901 (2020).
- [11] Y. Li, Y.-G. Peng, L. Han, M.-A. Miri, W. Li, M. Xiao, X.-F. Zhu, J. L. Zhao, A. Alù, S. H. Fan, and C.-W. Qiu, *Science* **364**, 170 (2019).
- [12] L. J. Xu, J. Wang, G. L. Dai, S. Yang, F. B. Yang, G. Wang, and J. P. Huang, *Int. J. Heat Mass Transfer* **165**, 120659 (2021).
- [13] R. L. Voti and M. Bertolotti, *Int. J. Heat Mass Transfer* **176**, 121098 (2021).
- [14] G. Q. Xu, Y. Li, W. Li, S. H. Fan, and C.-W. Qiu, *Phys. Rev. Lett.* **127**, 105901 (2021).
- [15] Y. Li, K.-J. Zhu, Y.-G. Peng, W. Li, T. Z. Yang, H.-X. Xu, H. Chen, X.-F. Zhu, S. H. Fan, and C.-W. Qiu, *Nat. Mater.* **18**, 48 (2019).
- [16] G. Q. Xu, K. C. Dong, Y. Li, H. G. Li, K. P. Liu, L. Q. Li, J. Q. Wu, and C.-W. Qiu, *Nat. Commun.* **11**, 6028 (2020).
- [17] L. J. Xu, J. P. Huang, and X. P. Ouyang, *Phys. Rev. E* **103**, 032128 (2021).
- [18] L. J. Xu, J. P. Huang, and X. P. Ouyang, *Appl. Phys. Lett.* **118**, 221902 (2021).
- [19] J. R. Willis, *Wave Motion* **3**, 1 (1981).
- [20] G. W. Milton and J. R. Willis, *Proc. R. Soc. A* **463**, 855 (2007).
- [21] C. F. Sieck, A. Alù, and M. R. Haberman, *Phys. Rev. B* **96**, 104303 (2017).
- [22] R. Pernas-Salomón and G. Shmuel, *Phys. Rev. Applied* **14**, 064005 (2020).
- [23] Y. Meng, Y. R. Hao, S. Guenneau, S. B. Wang, and J. Li, *New J. Phys.* **23**, 073004 (2021).
- [24] D. Torrent, O. Poncelet, and J.-C. Batsale, *Phys. Rev. Lett.* **120**, 125501 (2018).
- [25] M. Camacho, B. Edwards, and N. Engheta, *Nat. Commun.* **11**, 3733 (2020).
- [26] See Supplemental Material at <http://link.aps.org/supplemental/10.1103/PhysRevLett.128.145901> for detailed discussions, which includes Refs. [27–29].

- [27] D. D. Joseph and L. Preziosi, *Rev. Mod. Phys.* **61**, 41 (1989).
- [28] B.-D. Nie and B.-Y. Cao, *Int. J. Heat Mass Transfer* **135**, 974 (2019).
- [29] M. Gandolfi, G. Benetti, C. Glorieux, C. Giannetti, and F. Banfi, *Int. J. Heat Mass Transfer* **143**, 118553 (2019).
- [30] Y. Li, X. Y. Shen, Z. H. Wu, J. Y. Huang, Y. X. Chen, Y. S. Ni, and J. P. Huang, *Phys. Rev. Lett.* **115**, 195503 (2015).
- [31] Y. Li, J. X. Li, M. H. Qi, C.-W. Qiu, and H. S. Chen, *Phys. Rev. B* **103**, 014307 (2021).
- [32] M. Y. Wong, C. Y. Tso, T. C. Ho, and H. H. Lee, *Int. J. Heat Mass Transfer* **164**, 120607 (2021).
- [33] J. P. Huang, *Theoretical Thermotics: Transformation Thermotics and Extended Theories for Thermal Metamaterials* (Springer, Singapore, 2020).
- [34] S. Yang, J. Wang, G. L. Dai, F. B. Yang, and J. P. Huang, *Phys. Rep.* **908**, 1 (2021).
- [35] Y. Li, W. Li, T. C. Han, X. Zheng, J. X. Li, B. W. Li, S. H. Fan, and C.-W. Qiu, *Nat. Rev. Mater.* **6**, 488 (2021).